

¹ **Relative Detection Efficiency of the World** ² **Wide Lightning Location Network**

M. L. Hutchins¹, R. H. Holzworth¹, J. B. Brundell², and C. J. Rodger³

J. B. Brundell, UltraMSK.com, 7 Gowan Close, Waverley, Dunedin, 9013, New Zealand.
(james@brundell.co.nz)

R. H. Holzworth, Department of Earth and Space Sciences, University of Washington,
Box 351310, Johnson Hall 070, Seattle, WA 98105, USA. (bobholz@ess.washington.edu)

M. L. Hutchins, Department of Earth and Space Sciences, University of Washington, Box
351310, Johnson Hall 070, Seattle, WA 98105, USA. (mlhutch@uw.edu)

C. J. Rodger, Department of Physics, University of Otago, PO Box 56, Dunedin, 9016,
New Zealand. (crodger@physics.otago.ac.nz)

¹Department of Earth and Space Sciences,
University of Washington, Seattle,
Washington, USA

²UltraMSK.com, Dunedin, New Zealand

³Department of Physics, University of
Otago, Dunedin, New Zealand

3 Using the detected energy per strokes of the World Wide Lightning Lo-
4 cation Network (WWLLN) we calculate the relative detection efficiency for
5 the network as if it had a uniform detection efficiency. The model uses the
6 energy statistics of located strokes to determine which stations are sensitive
7 to what stroke energies. We are then able to estimate the number of strokes
8 that may be missing from any given regions as compared to the best, most
9 sensitive regions of the WWLLN network. Stroke density maps can be cor-
10 rected with the knowledge of how sensitive various regions of the network
11 are operating.

12 This new model for the relative WWLLN detection efficiency compensates
13 for the uneven global coverage of the network sensors as well as variations
14 in very low frequency (VLF) propagation. The model gives a way to repre-
15 sent the global distribution of strokes as if observed by a globally uniform
16 network. The model results are analyzed in spatial and temporal regimes,
17 and the effects of a single VLF detector going offline are investigated in ar-
18 eas of sparse and dense detector coverage. The results are also used to show
19 spatial, temporal and energy distributions as seen by the detection efficiency
20 corrected WWLLN.

1. Introduction

21 The World Wide Lightning Location Network (WWLLN) has been generating
22 global lightning locations since 2004 [Rodger *et al.*, 2006, 2009a]. Since then the
23 network has grown from 18 stations to over 60 as of August 2012. Additional sta-
24 tions have greatly improved the ability of WWLLN to locate progressively weaker
25 strokes [Rodger *et al.*, 2009a; Abarca *et al.*, 2010]. However the WWLLN network does
26 not observe lightning with the same detection efficiency everywhere. This is due to
27 variable WWLLN station coverage and the strong affect on very low frequency (VLF)
28 radio propagation from orography and ionospheric conditions along the great circle
29 path of a wave. This paper demonstrates a technique which uses only data collected
30 by the WWLLN network itself, to estimate the relative detection efficiency of each 5°
31 x 5° pixel over the earth compared to the best average WWLLN detection efficiency.
32 For instance, the lightning stroke density over central Africa, where WWLLN station
33 density is sparse, can now be compared to the region of the Earth with the best
34 detection efficiency, such as North America. This paper does not provide an absolute
35 detection efficiency calculation.

36 WWLLN (see <http://wwlln.net>) determines the location for nearly all lightning
37 producing storms around the globe in real time [Jacobson *et al.*, 2006]. The network
38 uses VLF radio wave receivers distributed around the globe to identify the time of
39 group arrival (TOGA) for the wave packets from individual lightning-produced spher-
40 ics [Dowden *et al.*, 2002]. A central processor combines the TOGAs to determine the
41 source locations over the spherical Earth. The TOGA of the VLF wave packet devel-

oped by *Dowden and Brundell* [2000], is used rather than “trigger time” to produce more uniform arrival times across the network. Stroke locations are determined using the TOGAs with a time of arrival algorithm over the spherical earth (see *Rodger et al.* [2009a, b]). Knowledge of global stroke locations, with high temporal and spatial accuracy is beneficial for both scientific and technical uses. WWLLN lightning location data have recently been used for advances in space science [*Lay et al.*, 2007; *Kumar et al.*, 2009; *Collier et al.*, 2009; *Holzworth et al.*, 2011; *Jacobson et al.*, 2011], meteorology [*Price et al.*, 2009; *Thomas et al.*, 2010], detailed lightning physics [*Connaughton et al.*, 2010], and volcanic eruption monitoring [Doughton, 2010].

As of April 2012 WWLLN consisted of 60 VLF stations distributed around the world, with more stations continuously being added to the network. The network improves in accuracy and detection efficiency with increased stations; for example an increase in the number of WWLLN stations from 11 in 2003 to 30 in 2007 led to a $\sim 165\%$ increase in the number of lightning strokes located [*Rodger et al.*, 2009a]. As of 2011 the network located 61% of strokes to <5 km and 54% to $<15 \mu s$ with an estimated detection efficiency of about 11% for cloud to ground flashes and $>30\%$ for higher peak current flashes over the Continental United States [*Hutchins et al.*, 2012b; *Abarca et al.*, 2010; *Rodger et al.*, 2009a].

A concern for all VLF networks is the non-uniform propagation of VLF waves due to changing ionospheric and surface conditions; this is true for networks monitoring lightning produced VLF signals like WWLLN, or those monitoring fixed-frequency communication transmitters like AARDDVARK [*Clilverd et al.*, 2009]. During the

64 day there is a larger ionospheric electron density at lower D-region altitudes. This
65 causes the range of electron-neutral collision frequencies to overlap with the range of
66 spheric wave frequencies, increasing the attenuation rate of the spherics. This increase in
67 electron number density is also seen in the change of the reference ionospheric height,
68 h' [*Wait and Spies*, 1960], during the day ($h' = 74$ km) compared to during the night
69 ($h' = 87$ km). There is a similar change in attenuation over the path of the spheric
70 from the differences in the conductivity of the oceans (4 S/m), continents (10^{-2} –
71 10^{-4} S/m), and Antarctic/Arctic ice (10^{-5} S/m). The many path parameters for a
72 given spheric result in a highly variable attenuation [*Volland*, 1995].

73 Thus, independently determining the real-time detection efficiency has always been
74 a challenging topic. Several studies have been conducted comparing the network to
75 other ground based networks or satellite measurements [*Lay et al.*, 2004; *Jacobson*
76 *et al.*, 2006; *Rodger et al.*, 2009a; *Abarca et al.*, 2010; *Abreu et al.*, 2010]. These studies
77 tend to be limited in either scope or in time due to the availability of data from
78 other networks. Past work by *Rodger et al.* [2006] attempted to determine the global
79 detection efficiency of WWLLN using a theoretical model linked to observations from
80 a ground based commercial lightning network in New Zealand. In this paper a new
81 method is developed for determining the relative detection efficiency of WWLLN
82 based upon the recent network advancement of measuring the radiated energy of
83 detected strokes [*Hutchins et al.*, 2012a].

84 Developing a model of detection efficiency expands the capabilities and uses for
85 WWLLN. In particular a model that does not rely on external comparisons to other

86 networks or sensors is critical for obtaining a dynamic global view of network per-
87 formance. Such a view will enable the network to be used with more confidence in
88 areas of lower coverage and enable the network to be utilized with uniform detection
89 efficiency in work requiring lightning rates and densities. This uniform performance
90 will allow for more accurate studies of global phenomena such as the short time
91 (<10 minute) variability of the global electric circuit, comparative lightning clima-
92 tology between regions, and production rate estimations of transient luminous events
93 and terrestrial gamma ray flashes. The detection efficiency model can combine with
94 the measurements of stroke energy and regional absolute detection efficiency studies
95 to advance research in global effects of lightning such as estimating the total spheric
96 energy transferred to the magnetosphere in the form of whistler waves.

1.1. Calculating the Radiated Stroke Energy

97 Every WWLLN spheric packet includes the TOGA and a measure of the root mean
98 square (RMS) electric field of the triggered waveform. The RMS electric field is taken
99 in the 6-18 kHz band over the triggering window of 1.33 ms. The U.S. Navy Long
100 Wave Propagation Capability (LWPC) code described by *Ferguson* [1998] is utilized
101 to model the VLF propagation from each located stroke to determine the necessary
102 stroke energy to produce the measured RMS electric field (in the VLF band) at each
103 WWLLN station. Using the measured RMS field at each station, the radiated energy
104 of each detected stroke is found. In 2010 WWLLN observed a global median stroke
105 energy of 629 J, with a 25% average uncertainty in the measured energy. The global

106 and regional distribution of energy is shown in Figure 1a. Of all the detected strokes
107 97% have corresponding energy values. [*Hutchins et al.*, 2012a]

108 In Figure 1a the statistical error bars (Poisson statistics) are not plotted as they
109 would be on the order, or smaller than, the line width. It is important to note that
110 the distribution of strokes in each region is lognormal [*Hutchins et al.*, 2012a] with
111 the main differences in the total strokes detected and the median energy, which is
112 399 J, 1101 J, and 798 J for the Americas (-180° E to -60° E), Africa (-60° E to 60°
113 E), and Asia (60° E to 180° E) respectively. An overall lower detection efficiency over
114 Africa, particularly for low energy strokes, causes median energy to be higher than
115 the other regions. Along with each region the energy distribution is lognormal from
116 an hourly time scale to the annual distribution. In Figure 1b the annual lognormal
117 distribution is shown with a monthly, daily, and hourly distribution. It is not until
118 the hourly distribution that the errors are noticeable, and the distribution is still
119 fairly lognormal.

2. Minimum Detectable Energy

120 The first step in calculating the relative detection efficiency for the entire network is
121 working out the minimum stroke energy that WWLLN can detect at a given location
122 and time. This process starts by finding the detection threshold at each station,
123 converting it to an energy value at each location in the world, and then selecting
124 the minimum detectable network energy at every location based on the minimum

125 observable energy from each station. Detailed examples of how this works are given
126 next for single stations and for the network as a whole.

2.1. Station Threshold

127 At each WWLLN station the threshold for triggering on an event (and calculating
128 the TOGA at that station) is dynamically selected depending on observed activity
129 at that station as described in Section 5.3 of *Rodger et al.* [2006]. Presently every
130 WWLLN station automatically adjusts the triggering threshold to send an average of
131 3 packets per second to the central processor. For instance, when a station is detecting
132 many strokes, the trigger threshold at that station is raised to maintain a steady flow
133 of sferic packets. Since a station can only measure the electric (or magnetic) field
134 of an event it cannot accurately discern whether a sferic comes from a nearby weak
135 stroke or a strong distant stroke; for the case of the strongest lightning strokes the
136 discharge could be on the other side of the Earth from the WWLLN station and still
137 be detected.

138 The effect of the variable trigger threshold can be seen in Figure 2a which is a
139 2 - D histogram of number of strokes with specific RMS field and UT values on 15
140 June 2010 for the Dunedin, New Zealand, WWLLN station (-45.864° N, 170.514°
141 E). In Figure 2b the threshold can be seen as the lower cutoff of the triggered RMS
142 field strength distribution, the station threshold is reconstructed hourly as the 5th
143 percentile value (red line) of the distribution. The threshold value varies relatively
144 slowly over the course of the day.

2.2. Station Minimum Detectable Energy

145 The minimum detectable energy (MDE) is the minimum energy a lightning stroke
146 must radiate in the VLF to be detected by WWLLN or a WWLLN station (denoted
147 network MDE and station MDE respectively). The MDE is a function of space,
148 time and station threshold. Each station has a variable threshold which varies slowly
149 during the day. Slow ionospheric variations can also affect the MDE by changing the
150 VLF attenuation and detected RMS field.

151 Every hour the reconstructed minimum RMS field necessary to trigger an event
152 is calculated and converted to a stroke energy. To make this conversion the same
153 method as calculating the radiated energy per stroke is used as described in *Hutchins*
154 *et al.* [2012a]. This results in a station MDE for every point on a $5^\circ \times 5^\circ$ global grid,
155 which is the stroke energy necessary at that location to trigger a TOGA calculation
156 at the given station. As an example the map of the MDE for our Dunedin station
157 (data shown in Figure 2) is shown in Figure 3. Figure 3 applies only to strokes
158 detected at this one station in Dunedin, a similar map can be generated for every
159 WWLLN station. The high MDEs in Figure 3 over the Antarctic, Western Africa,
160 and Greenland are due to the high VLF attenuation over ice, and imply that Dunedin
161 is very unlikely to detect strokes with energy less than the MDE if they were to occur
162 in these regions.

163 In order to locate a stroke, WWLLN requires TOGA values from at least five
164 stations in order to conduct adequate fit error analysis. For every $5^\circ \times 5^\circ$ grid cell all
165 of the minimum stroke energies from currently active WWLLN stations are ordered.

166 An example for one cell is shown in Table 1. The 5th lowest from this list is used as
167 the network MDE, because at least five stations can trigger on that energy value. In
168 other words, WWLLN cannot detect a stroke until it has a radiated energy which is
169 above the trigger threshold at five or more WWLLN stations. A map of the network
170 MDE is shown in Figure 4. Similar to the station MDE map for our Dunedin station,
171 Figure 3, there are higher MDE values above the Arctic and Antarctic ice regions.

172 Regions of the network with higher MDE, from either increased VLF attenuation,
173 station thresholds or sparse coverage, preferentially detect a higher ratio of energetic
174 strokes to all strokes. For example southern Africa has a higher MDE than other
175 regions and the median energy, shown in Figure 1a is correspondingly higher. Con-
176 versely regions with low MDE, such as the Americas, show a lower median energy.

3. Relative Detection Efficiency

177 The next important step in calculating the relative detection efficiency is to estab-
178 lish the relationship between the network MDE and relative detection efficiency. The
179 relative detection efficiency is a measure of how well a given location in the network
180 is being observed relative to the best region in the network. In a given grid cell
181 the network MDE is compared to the total WWLLN energy distribution of the past
182 seven days. For a given network MDE value the fraction of total strokes above the
183 network MDE gives the relative detection efficiency. The past seven day distribution
184 is used as the base distribution in order to average over diurnal and station perfor-
185 mance variations. This lognormal base distribution is assumed to be representative

186 of a single universal distribution of stroke energies that could be detected globally by
187 a uniform WWLLN.

188 For example, if a location has an network MDE of 100 J, then the number of strokes
189 in the past seven days above 100 J (grey area, Figure 5a) is compared to the total
190 number of strokes which were located in that location in those seven days. In this
191 case the grey area has a count of 2.6×10^6 strokes and the total number of WWLLN
192 strokes is 2.9×10^6 strokes, so for this network MDE of 100 J the relative detection
193 efficiency is 90%. Similarly if a location has a high network MDE value there will be
194 few strokes with energy above it, so it will have a low relative detection efficiency.

195 This calculation is done for a range of hypothetical network MDE values which
196 produces a curve shown in Figure 5b, to give the relationship between MDE and
197 relative detection efficiency. This relationship is established once per day, and it is
198 used to produce hourly maps of relative detection efficiency for that day. This is done
199 by taking the hourly maps of network MDE and applying this relation to every 5°
200 x 5° point on the globe for every hour to convert the network MDE to the relative
201 detection efficiency.

202 The relative detection values given by this process are only in reference to the energy
203 distribution of the past seven days as seen by WWLLN. If a region has a relative
204 detection efficiency of 100% then the region is able to detect all of the detected
205 stroke energies present in the 7-day network energy distribution. The corrections
206 from the relative detection efficiency maps can be used to generate lightning density
207 distributions as though WWLLN had global uniform coverage at the same level as

208 that of the best parts of the network. This is because the method does not correct the
209 network to absolute stroke counts, just to a globally uniform performing WWLLN.

3.1. Hourly Maps

210 A set of four hourly maps from 15 June 2010 showing the networks relative de-
211 tection efficiency every 6 hours from 00 UTC to 18 UTC is presented in Figure 6.
212 Stations that were operational for the hour shown are displayed in white and sta-
213 tions that were not operational are black (operational taken to triggering > 500
214 strokes/hour). The four major competing effects on the detection efficiency are the
215 day/night terminator, local stroke activity, station density, and station performance.
216 The day/night terminator effect can be seen as it moves from 00 UTC (Figure 6a)
217 through 18 UTC (Figure 6d). An increase in local stroke activity in North Ameri-
218 can afternoon (Figure 6a) causes a decrease in detection efficiency as nearby stations
219 raise their triggering thresholds. Station density is coupled with station performance,
220 since when a station is not operating optimally it has a similar effect as removing
221 that station, the effect of station performance is discussed in a later section.

222 Figure 7 shows the daily relative detection efficiency from the average of the hourly
223 maps, here grey stations were only operational part of the day. This average map
224 is more representative of the relative detection efficiency for the day and it shows
225 behavior that is expected based on the distribution of stations: lower detection effi-
226 ciency over most of Africa with higher detection efficiency over and around the Pacific
227 and North America. The low detection efficiency over Antarctica, parts of Siberia,
228 and Greenland are due to the high attenuation of VLF propagating subionospheri-

229 cally over ice. Conversely the high detection efficiency over North America, Western
230 Europe, and Oceania, are due to the high station density and low attenuation of
231 VLF over ocean. In order to prevent unphysical overcorrections, a minimum relative
232 detection efficiency of 5% has been set for all of the relative detection efficiency maps.

4. Analysis

4.1. Distribution Changes

233 As shown in the previous sections the relative detection efficiency values in a given
234 day are derived from the WWLLN observed stroke energy distribution from the
235 previous seven days, this allows for direct comparisons within a day and for nearby
236 days, but it does not take into account the changing distribution from changes in the
237 network. As more stations are added to the network additional low-energy strokes
238 will be detected and the overall energy distribution will shift towards lower values.
239 When the overall network distribution changes between years, then for a given region
240 the relative detection efficiency can change even if that region of the network has
241 detected the same distribution of strokes.

242 One way to examine the change in the distribution of energy is to examine the
243 temporal variability of the median of the global WWLLN energy distribution, the
244 median of the seven day distribution is shown in Figure 8. The median energy varies
245 from the three year median by 52% with the daily median value ranging from 400 J
246 to 2000 J. The variability is caused by ionospheric changes not accounted for in the
247 ionospheric model used. Several jumps in the median energy (e.g., Dec 2009 and
248 Dec 2010) are caused by changes in the primary calibrated WWLLN station (see

249 *Hutchins et al.* [2012a]) such as gain changes. The slow increase to Aug 2011 was
250 due to a change of the primary calibrated station from the Dunedin, New Zealand
251 station to the Scott Base, Antarctica station. It is important to note that since the
252 detection efficiency is relative to the past seven days, the relatively slow changes in
253 median energy do not strongly affect the detection efficiency and highlight how the
254 relative detection efficiency cannot correct for absolute overall network performance.

4.2. Temporal Variability

255 The evolution of the network can be seen as an increase in the global average relative
256 detection efficiency, calculated by averaging all grid cells of the each hourly maps for
257 a day. While no region can have a relative detection efficiency over 100%, as regions
258 improve with more stations they will approach 100% and increase the global average
259 detection efficiency. The global average relative detection efficiency from April 2009
260 through October 2011 is shown as the green line in Figure 9. In the Figure the
261 total number of operational stations is shown as the black line, and it has a strong
262 correlation to the global averaged detection efficiency with a correlation value of 0.86.
263 With more stations strategically added to the network the 7-day energy distribution
264 will also change to include more low energy strokes and increase the average relative
265 detection efficiency.

266 While Figure 9 shows an overall increase in the number of network stations and
267 hence detection efficiency, Figure 10 shows similar curves for just low-latitude regions
268 (-30° N to 30° N, blue), a single location near Florida (-85° E, 30° N, red), and a sin-
269 gle location near South Africa (25° E, -20° N, green). Removing high latitude regions

270 increases the overall detection efficiency but does not change the overall upward trend
271 shown by the blue curve in Figure 10. When the region near Florida is examined it
272 can be seen that it remains fairly close to 1.0 for the entire dataset, with downward
273 trends during local summer months due to increased local lightning activity. The
274 region near South Africa has a steady increase in detection efficiency except during
275 a large drop out which occurred in the middle of 2011, caused by one of the African
276 stations going offline. This shows the global detection efficiency tracks the network
277 as a whole, but it cannot be used as an accurate proxy for smaller spatial scales.

278 The local time variability over the region near Florida is shown in black in Figure 11
279 and shows a total variability of about 4.9%. The largest drop in the relative detection
280 efficiency occurs in the afternoon, near the peak in local lightning activity at 3pm.
281 This drop is due to the nearby stations raising their detection threshold in response to
282 detecting more local strokes. For this location the effects of local activity dominates
283 over the expected day/night effect due to changes in VLF propagation.

284 The variability for the region near South Africa is shown as the dotted line in
285 Figure 11, there is a total variability of 25.5%. There is an overall decrease in relative
286 the detection efficiency during the day when the sferics are propagating over the
287 continent. The best in relative detection efficiency occurs in the middle of the night
288 when the stations in Africa have less nearby activity and sferics are able to propagate
289 more readily under a night ionosphere. Compared to the Florida region there is a
290 much higher dependence on day and night conditions as well as a much wider range
291 of variability.

4.3. Station Outage Effects

292 While the overall performance of the network trends along with the total number
293 of stations, the effects a single station turning on or off can have an effect on a large
294 region of the global but only small effect on the network as a whole. To test the
295 influence of single stations a day of data was randomly selected, 16 June 2010, and
296 the entire data were reprocessed with just the Honolulu, Hawaii station (-158°E ,
297 21°N) removed from the raw data and again with just the Maitri, Antarctica station
298 (12°E , -71°N) removed. The maps of the daily average with and without these
299 stations are shown in Figure 12. For Hawaii the change is fairly local to its region
300 in the Northeast Pacific Ocean, but leads to little effect across the entire network.
301 In the case of Maitri there is a larger effect since it is located in a region of sparse
302 detector coverage and covers much of the southern Atlantic.

303 The daily average global relative detection efficiency dropped from 64% to 63%
304 without Hawaii and from 64% to 53% without Maitri. The detection efficiency in the
305 grid cell over Hawaii dropped from 85% to 78% and from 45% to 7.4% in the grid
306 cell over Maitri. A plot of the total change between the daily averages in Figure 12
307 is shown in Figure 13.

5. Results

308 The detection efficiency model can be applied to global maps of stroke density to
309 estimate, or correct for the global stroke density which would be seen if WWLLN
310 had a uniform spatial and temporal coverage. This does not correct for the overall

311 absolute detection efficiency (11% for CG flashes in the United States, see *Abarca*
312 *et al.* [2010]), rather it corrects for the areas with less WWLLN coverage. The hourly
313 stroke density plots are corrected by dividing the counts in each grid cell by the
314 relative detection efficiency of that cell. For example a grid cell with 100 strokes and
315 an efficiency of 80% would be corrected to 125 strokes. The stroke density from 2011,
316 Figure 14, had the model corrections applied hourly with the condition that a $5^\circ \times 5^\circ$
317 grid cell needed at least two strokes to have a correction applied. A second condition
318 was that a minimum relative detection efficiency of 5% was set for the model.

319 The total number of strokes for 2010 was 1.4×10^8 (4.4 strokes/second), and after
320 applying the model the total was 2.0×10^8 strokes (6.3 strokes/second). In 2011 the
321 total number of strokes was 1.5×10^8 (4.8 strokes/second) with a model-corrected
322 value of 1.9×10^8 (6.0 strokes/second). In 2010 63% of the global area between
323 $\pm 60^\circ$ latitude had a relative detection efficiency of at least 80% and in 2011 this area
324 increased from 66% to 72%. If we assume that the global lightning flash rate was a
325 constant 46 flashes/second as determined by satellite measurements using the Optical
326 Transient Detector and Lightning Imaging Sensor [*Cecil et al.*, 2011; *Christian et al.*,
327 2003] for both years, this would imply a corrected global absolute detection efficiency
328 for cloud to ground and in-cloud flashes of 13.7% for 2010 and 13.0% in 2011.

329 The corrected yearly density is shown in Figure 15, aside from the overall increase
330 in number counts the important feature is the relative count rates over the US, Africa,
331 and Southeast Asia. In the uncorrected Figure 14 the peak stroke density in Asia
332 and America are similar while Africa is about ~ 1 -10% of these values (also shown

333 in Figure 1a). In the corrected maps we can see that the peak density in Africa
334 is much closer in magnitude to that seen for America and Asia, and the relative
335 densities match the distributions seen by OTD (see *Christian et al.* [2003] Figure 4).
336 The total increase in stroke counts is shown in Figure 16 with the greatest increases
337 occurring over land, in particular central Africa.

6. Conclusion

338 A relative detection efficiency model is developed for WWLLN based on the
339 WWLLN observed stroke energy distribution. The model is examined on various
340 temporal scales as well as performance changes due to station outage effects. The
341 model is applied to the 2011 WWLLN dataset to produce a corrected map of stroke
342 activity, matching the expected characteristics of satellite data. Work on comparing
343 distant regions is now possible as the network data can be corrected to a uniform
344 global level of performance. Future work will focus on achieving a model for absolute
345 detection efficiency.

346 Acknowledgments.

347 The authors wish to thank the World Wide Lightning Location Network
348 (<http://wwlln.net>), a collaboration among over 50 universities and institutions, for
349 providing the lightning location data used in this paper.

References

- 350 Abarca, S. F., K. L. Corbosiero, and T. J. Galarneau (2010), An evaluation of the
351 Worldwide Lightning Location Network (WWLLN) using the National Lightning
352 Detection Network (NLDN) as ground truth, *Journal of Geophysical Research*,
353 *115*(D18), 1–11, doi:10.1029/2009JD013411.
- 354 Abreu, D., D. Chandan, R. H. Holzworth, and K. Strong (2010), A performance
355 assessment of the World Wide Lightning Location Network (WWLLN) via com-
356 parison with the Canadian Lightning Detection Network (CLDN), *Atmospheric*
357 *Measurement Techniques*, *3*(4), 1143–1153, doi:10.5194/amt-3-1143-2010.
- 358 Cecil, D., D. Buechler, and R. Blakeslee, TRMM-based Lightning Climatology, in
359 *Proceedings of the 14th International Conference on Atmospheric Electricity -*
360 *ICAE*, Proceedings of the 14th International Conference on Atmospheric Electricity
361 - ICAE, ICAE, Rio de Janeiro, 2011.
- 362 Christian, H., et al. (2003), Global frequency and distribution of lightning as observed
363 from space by the Optical Transient Detector, *Journal of Geophysical Research*,
364 *108*(D1), 4005, doi:10.1029/2002JD002347.
- 365 Clilverd, M. a., et al. (2009), Remote sensing space weather events: the AARD-
366 DVARK network, *Space Weather*, *7*(4), doi:10.1029/2008SW000412.
- 367 Connaughton, V., et al. (2010), Associations between Fermi Gamma-ray Burst
368 Monitor terrestrial gamma ray flashes and sferics from the World Wide Light-
369 ning Location Network, *Journal of Geophysical Research*, *115*(A12), 1–14, doi:
370 10.1029/2010JA015681.

- 371 Collier, a. B., B. Delport, a. R. W. Hughes, J. Lichtenberger, P. Steinbach,
372 J. Öster, and C. J. Rodger, Correlation between global lightning and whistlers
373 observed at Tihany, Hungary, *Journal of Geophysical Research*, 114(A7), doi:
374 10.1029/2008JA013863, 2009.
- 375 Doughton, S., 2010: Faraway volcanic eruptions now detected in a flash. Seat-
376 tle Times, available from: [http://seattletimes.nwsourc.com/html/localnews/
377 2013733939_lightning22m.html](http://seattletimes.nwsourc.com/html/localnews/2013733939_lightning22m.html), (front page).
- 378 Dowden, R. L., and J. B. Brundell (2000), Improvements relating to the location of
379 lightning discharges, *Australia Patent*, 749713.
- 380 Dowden, R. L., J. B. Brundell, and C. J. Rodger (2002), VLF lightning location
381 by time of group arrival (TOGA) at multiple sites, *Journal of Atmospheric and
382 Solar-Terrestrial Physics*, 64(7), 817–830.
- 383 Ferguson, J. A. (1998), Computer Programs for Assessment of Long- Wavelength
384 Radio Communications, Version 2.0, *Tech. Rep. 3030*, Space and Naval Warfare
385 Systems Center, San Diego.
- 386 Holzworth, R. H., M. P. McCarthy, R. F. Pfaff, a. R. Jacobson, W. L. Willcockson,
387 and D. E. Rowland (2011), Lightning-generated whistler waves observed by probes
388 on the Communication/Navigation Outage Forecast System satellite at low lati-
389 tudes, *Journal of Geophysical Research*, 116(A6), 1–7, doi:10.1029/2010JA016198.
- 390 Hutchins, M. L., R. H. Holzworth, C. J. Rodger, and J. B. Brundell (2012a), Far-field
391 Power of Lightning Strokes as Measured by the World Wide Lightning Location
392 Network, *Journal of Atmospheric and Oceanic Technology*, 29, 1102–1110, doi:

393 10.1175/JTECH-D-11-00174.1.

394 Hutchins, M. L., R. H. Holzworth, C. J. Rodger, S. Heckman, and J. B. Brundell
395 (2012b), WWLLN Absolute Detection Efficiencies and the Global Lightning Source
396 Function, presented at European Geophysical Union General Assembly 2012, Vi-
397 enna, Austria.

398 Jacobson, A. R., R. Holzworth, J. Harlin, R. Dowden, and E. Lay (2006), Performance
399 Assessment of the World Wide Lightning Location Network (WWLLN), Using the
400 Los Alamos Sferic Array (LASA) as Ground Truth, *Journal of Atmospheric and*
401 *Oceanic Technology*, 23(8), 1082, doi:10.1175/JTECH1902.1.

402 Jacobson, a. R., R. H. Holzworth, R. F. Pfaff, and M. P. McCarthy (2011), Study of
403 oblique whistlers in the low-latitude ionosphere, jointly with the C/NOFS satellite
404 and the World-Wide Lightning Location Network, *Annales Geophysicae*, 29(5),
405 851–863, doi:10.5194/angeo-29-851-2011.

406 Kumar, S., A. Deo, and V. Ramachandran (2009), Nighttime D-region equivalent
407 electron density determined from tweek sferics observed in the South Pacific Region,
408 *Earth Planets Space*, 3(2), 905–911.

409 Lay, E. H., R. H. Holzworth, C. J. Rodger, J. N. Thomas, O. P. Jr., and R. L.
410 Dowden (2004), WWLL global lightning detection system: Regional validation
411 study in Brazil, *Geophysical Research Letters*, 31.

412 Lay, E. H., A. R. Jacobson, R. H. Holzworth, C. J. Rodger, and R. L. Dowden
413 (2007), Local time variation in land/ocean lightning flash density as measured by
414 the World Wide Lightning Location Network, *Journal of Geophysical Research*,

415 112(D13), 1–9, doi:10.1029/2006JD007944.

416 Price, C., M. Asfur, and Y. Yair (2009), Maximum hurricane intensity pre-
417 ceded by increase in lightning frequency, *Nature Geoscience*, 2(April), 2–5, doi:
418 10.1038/NGEO477.

419 Rodger, C. J., S. Werner, J. B. Brundell, E. H. Lay, N. R. Thomson, R. H. Holzworth,
420 and R. L. Dowden (2006), Detection efficiency of the VLF World-Wide Lightning
421 Location Network (WWLLN): initial case study, *Annales geophysicae*, 24, 3197–
422 3214.

423 Rodger, C. J., J. B. Brundell, R. H. Holzworth, E. H. Lay, N. B. Crosby, T.-Y.
424 Huang, and M. J. Rycroft (2009a), Growing Detection Efficiency of the World
425 Wide Lightning Location Network, *AIP Conference Proceedings*, pp. 15–20, doi:
426 10.1063/1.3137706.

427 Rodger, C. J., J. B. Brundell, and R. H. Holzworth (2009b), Improvements in the
428 WWLLN network: Improving detection efficiencies through more stations and
429 smarter algorithms, in *Japan Geoscience Union Meeting*, p. (Invited Oral), Chiba
430 City, Japan.

431 Thomas, J. N., N. N. Solorzano, S. A. Cummer, and R. H. Holzworth (2010), Polarity
432 and energetics of inner core lightning in three intense North Atlantic hurricanes,
433 *Journal of Geophysical Research*, 115(A00E15), 1–11, doi:10.1029/2009JA014777.

434 Volland, H. (1995), Longwave Sferic Propagation within the Atmospheric Waveguide,
435 in *Handbook of Atmosphericics Volume II*, edited by H. Volland, chap. 3, pp. 65–93,
436 CRC Press, Boca Raton.

437 Wait, J., and K. Spies (1960), Influence of earth curvature and the terrestrial magnetic
438 field on VLF propagation, *Journal of Geophysical Research*, 65(8), 2325–2331.

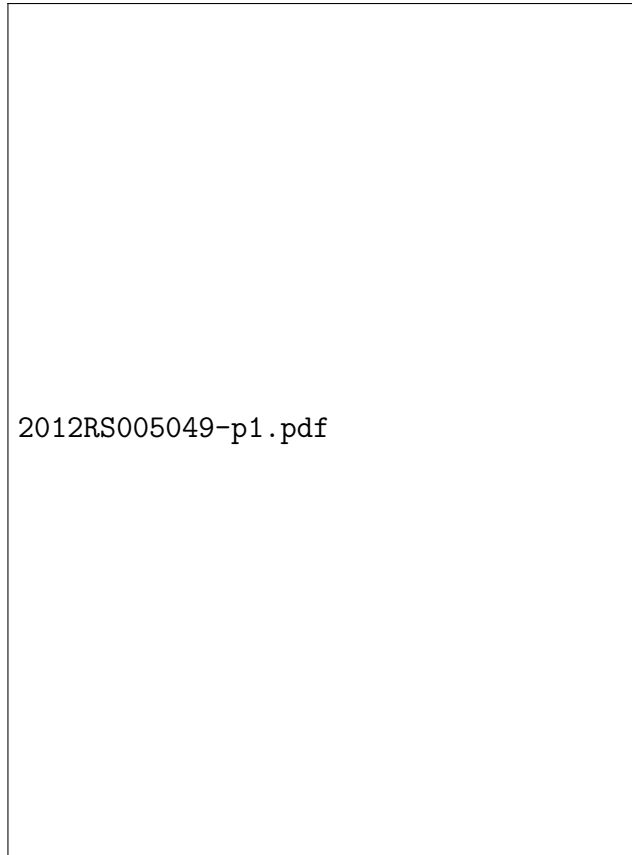
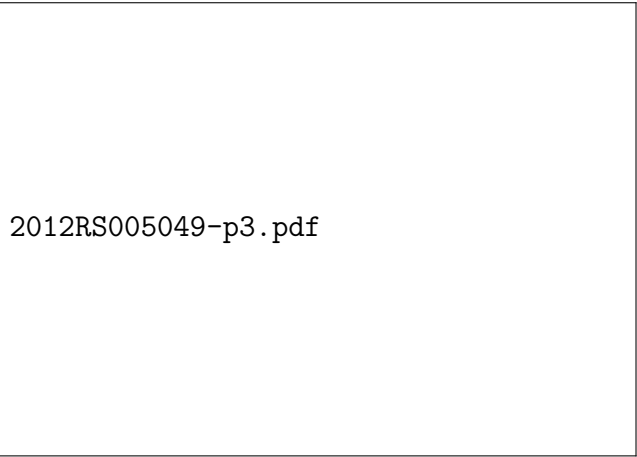


Figure 1. (a) WWLLN stroke energy distribution for the globe (black), the Americas (blue), Asia (green) and Africa/Europe (red). (b) WWLLN global stroke energy distribution for a year (2010), month (June 2010), day (15 June 2010), and hour (09 UTC 15 June 2010). Grey lines are statistical count errors.



2012RS005049-p2.pdf

Figure 2. (a) shows the evolution of the triggered RMS field strength distribution (in arbitrary units) for the Dunedin WLLN station with the red line showing the 5th percentile value. (b) shows the 9 UTC slice of the distribution, with the 5th percentile value marked (red line).



2012RS005049-p3.pdf

Figure 3. The minimum detectable energy (MDE) for the Dunedin station at 9 UTC on 15 June 2010. The regions of high MDE are due to poor VLF propagation over ice from those regions to Dunedin station. The white line shows the terminator.

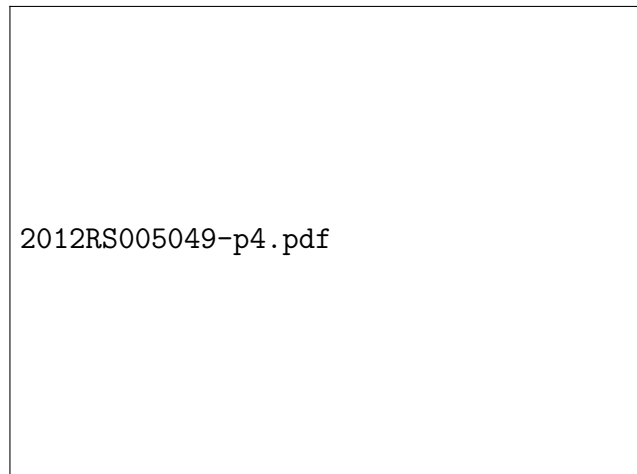


Figure 4. The minimum detectable energy (MDE) for the entire WWLLN network at 9 UTC on 15 June 2010.

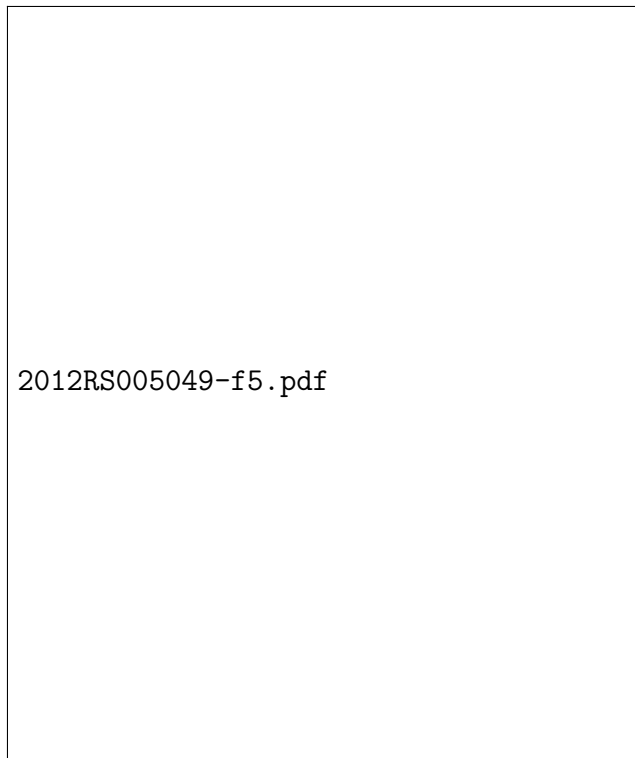


Figure 5. (a) The seven day energy distribution with the strokes above the MDE of 100 J shown in grey. The fraction of strokes above 100 J to total strokes gives a relative detection efficiency of 0.9, shown as a circle in (b). The fraction for all possible MDE values is shown as the curve in (b).



Figure 6. Relative detection efficiency maps for 00, 06, 12, and 18 UTC on 15 June 2010. Stations are shown as triangles with operational stations in white and non-operational in black. The minimum value of detection efficiency is set at 5% to prevent unphysical corrections.

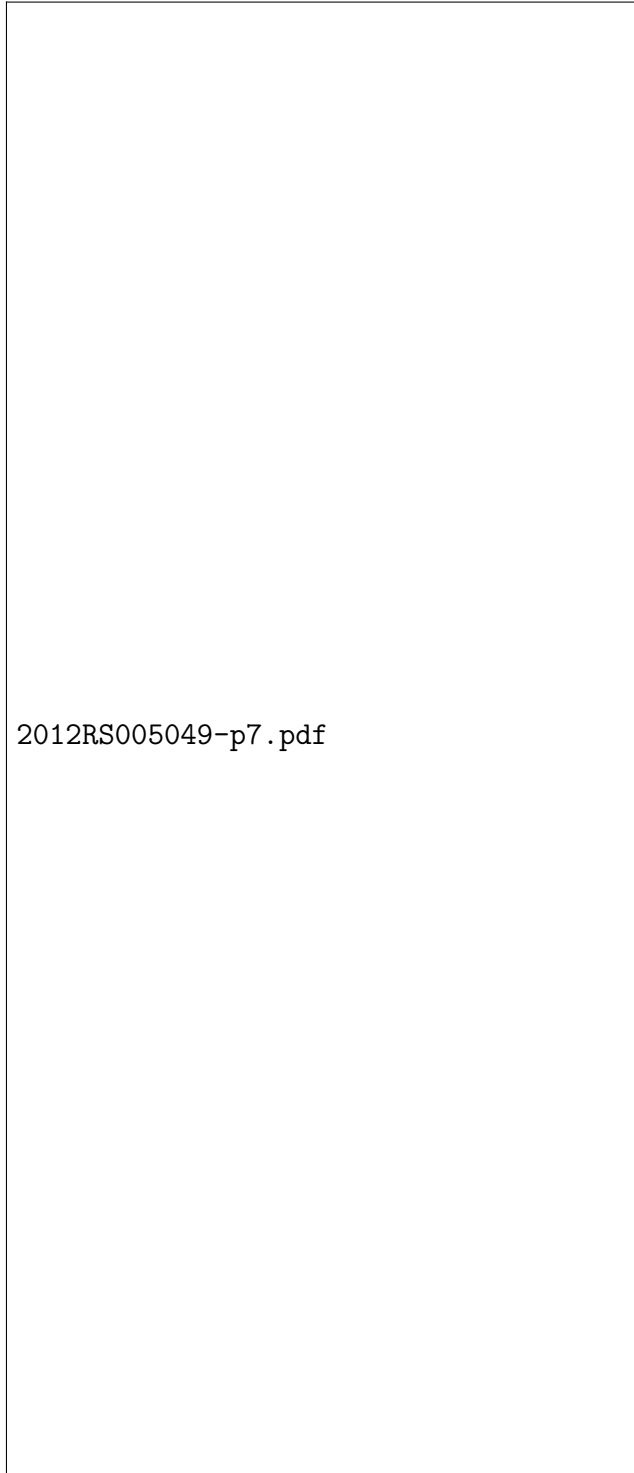


Figure 7. Daily average relative detection efficiency for 15 June 2010. Stations are shown as triangles with operational stations in white, non operational in black, and operational for part of the day in grey. The minimum value of detection efficiency is set at 5% to prevent

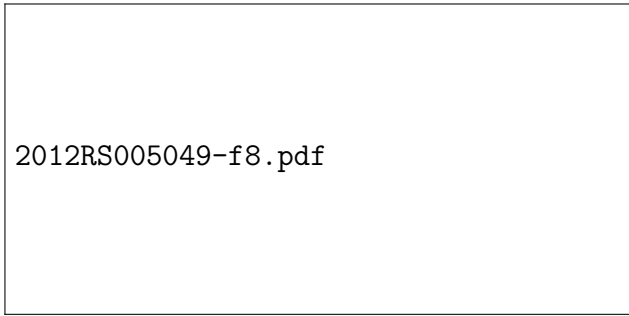


Figure 8. Median stroke energy of the 7-day distribution observed by WWLLN. The relative detection efficiency of the network is based on this 7-day energy distribution.

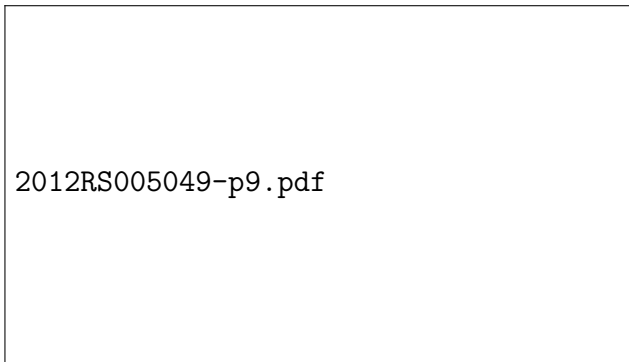


Figure 9. The number of WWLLN stations operating (black) and the global average relative detection efficiency (green) for April 2009 through October 2011.

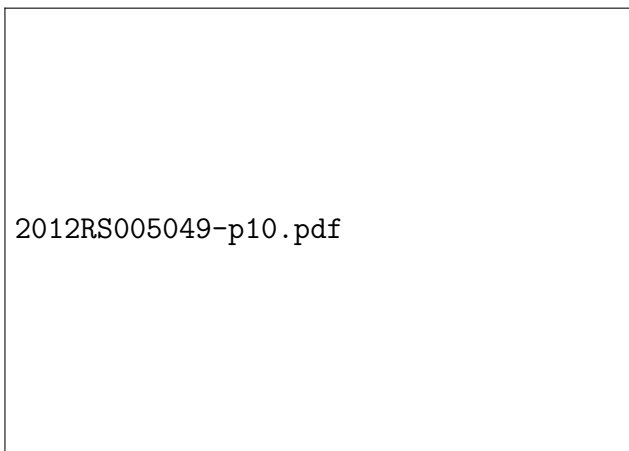


Figure 10. Daily variation of average detection efficiency for the globe (black), low-latitudes (-30° N to 30° N, blue), over Florida (-85° E, 30° N, red), and over South Africa (-25° E, -20° N, green).

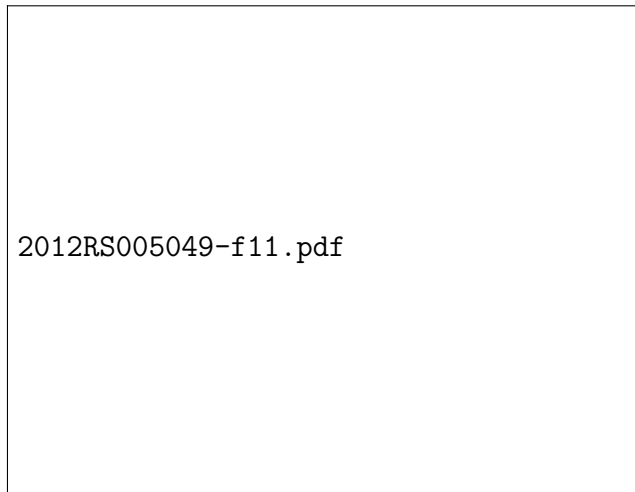


Figure 11. Average local time variation of detection efficiency over Florida (-85°E , 30°N , solid) and South Africa (-25°E , -20°N , dashed), from 2009-2011.

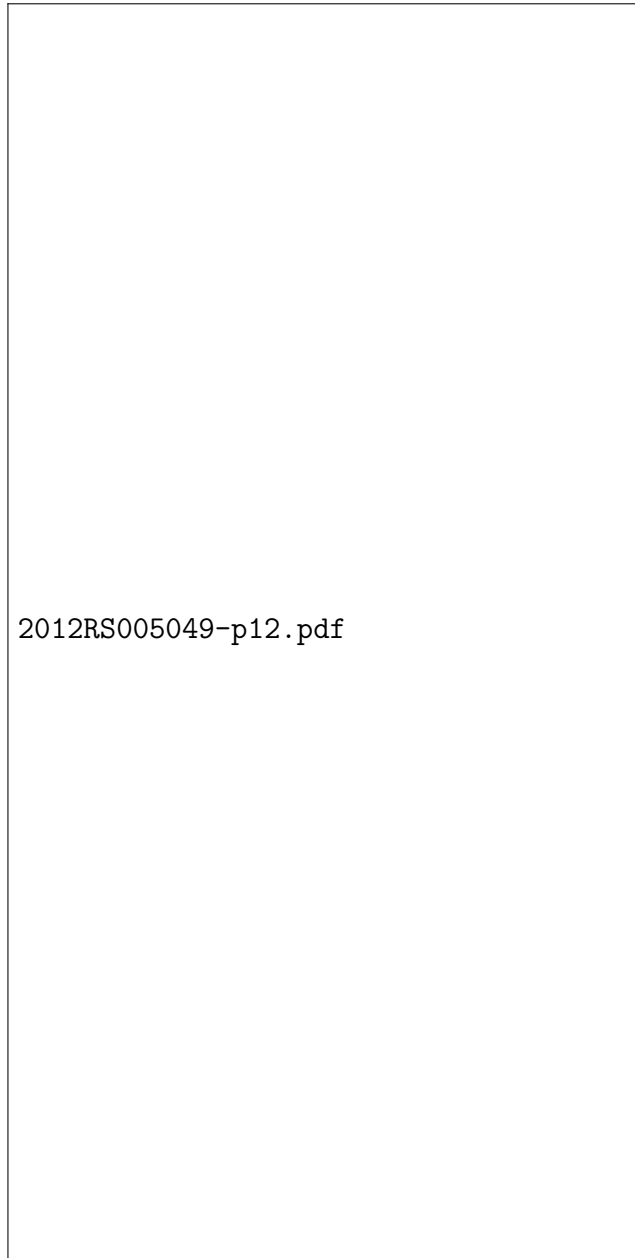
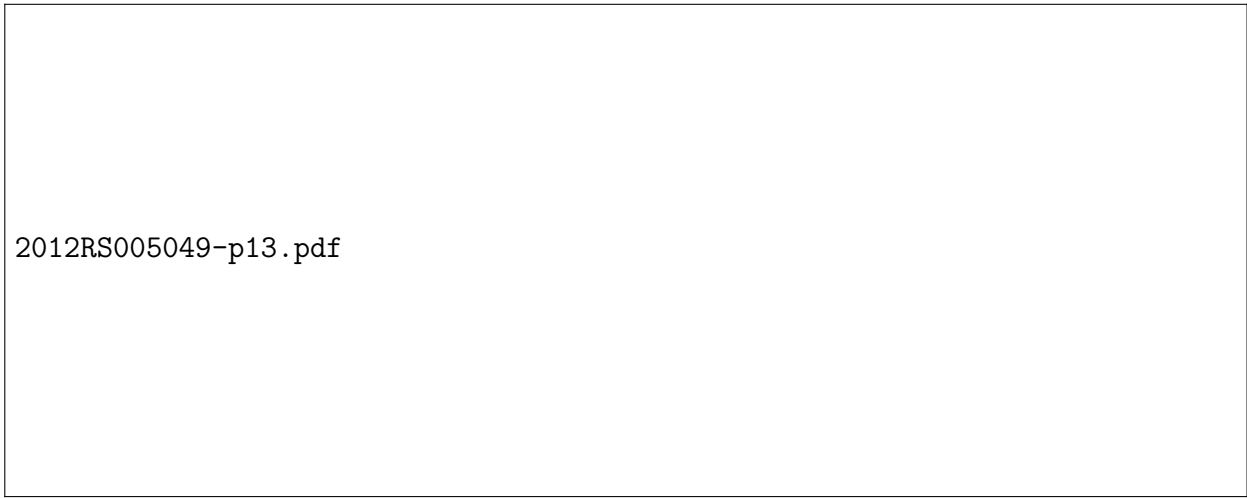
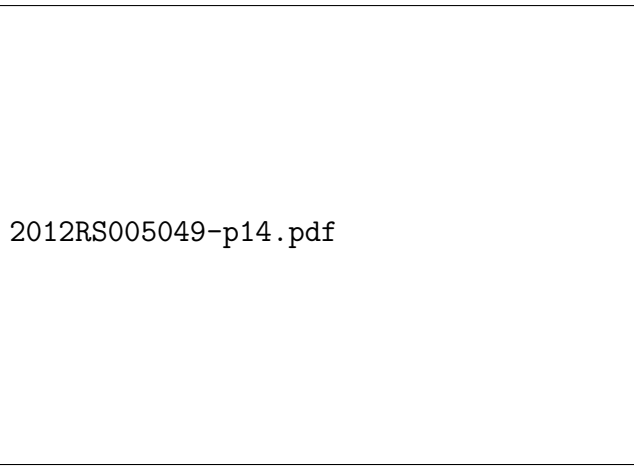


Figure 12. Relative detection efficiency map of 16 June 2010 for (a) the complete network, (b) the network with the Hawaii station (black star, -158°E , 21°N) removed, and (c) the network with Maitri station (black star, 12°E , -71°N) removed. Stations are shown as triangles with operational stations in white, non operational in black, and operational for part of the day in grey.



2012RS005049-p13.pdf

Figure 13. The difference in detection efficiency for 16 June 2010 with Hawaii (a) and Maitri (b) stations completely removed from processing.



2012RS005049-p14.pdf

Figure 14. The raw 2011 global stroke density measured by WWLLN.

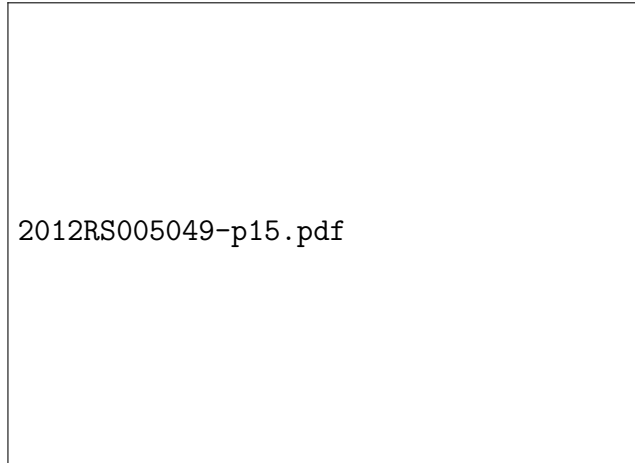


Figure 15. The 2011 global stroke density measured by WWLLN and corrected for the relative detection efficiency of the network. Note the large change in the African continent relative to Figure 14.

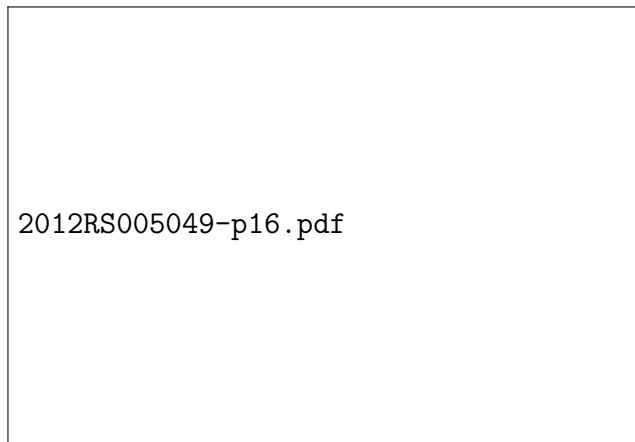
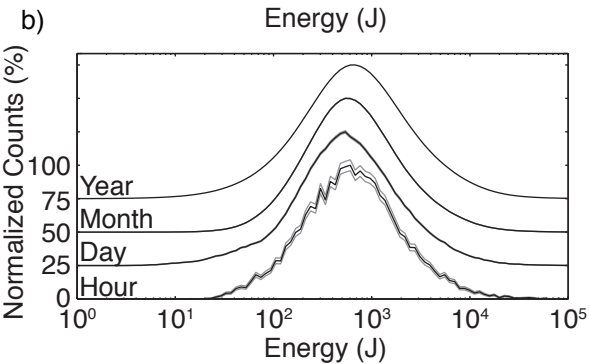
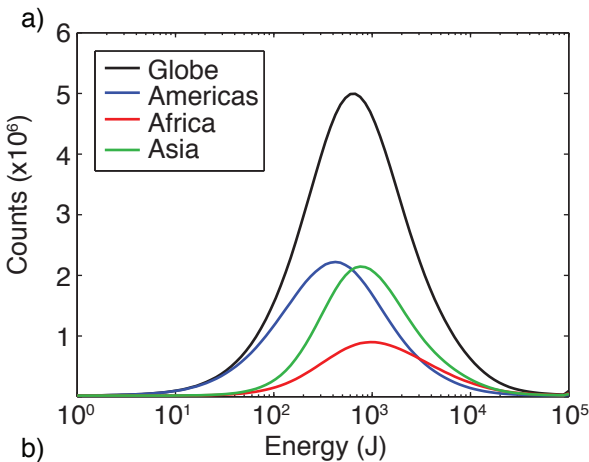
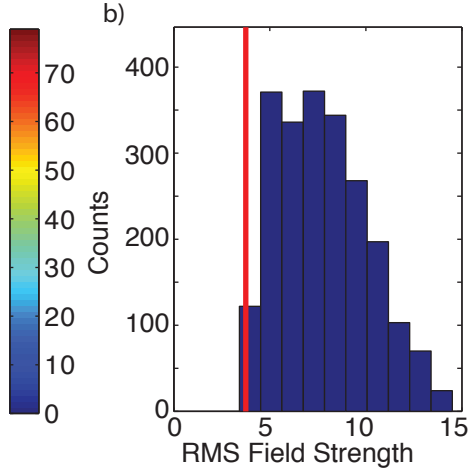
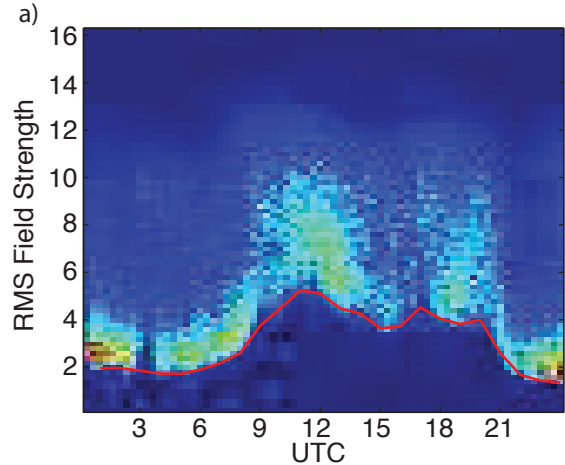


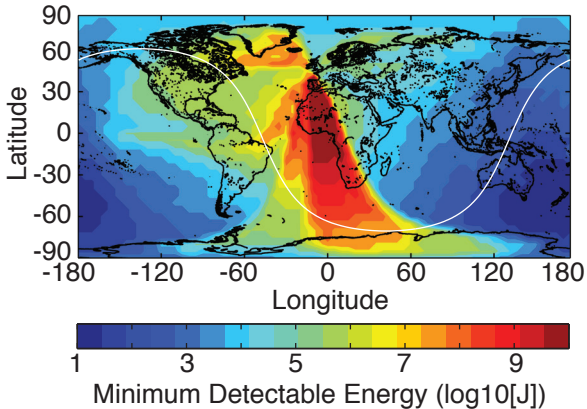
Figure 16. The increase in stroke density due to the relative detection efficiency corrections for 2011. Uncorrected and corrected stroke densities shown in Figure 14 and 15 respectively. The increase is plotted on the same scale as the previous two figures.

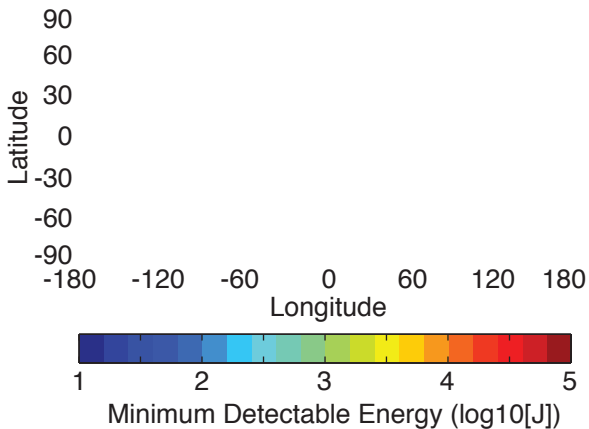
Table 1. Ordered list of station MDE values at -25°N , 20°E and 09 UTC on 15 June 2010. The fifth lowest value (in bold) is the network MDE at this location.

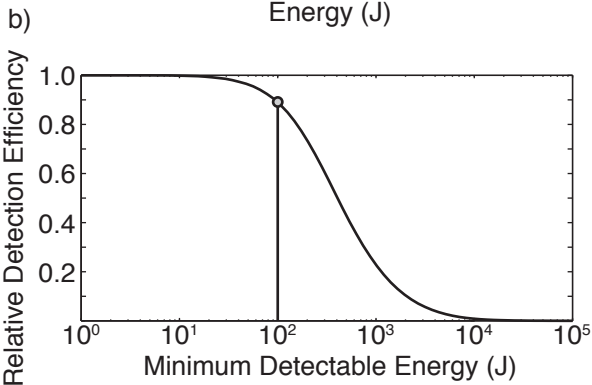
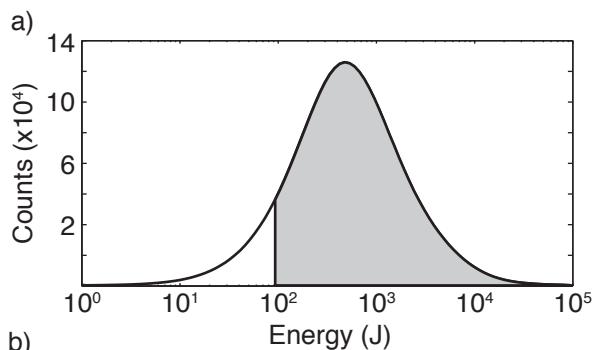
Station Name	MDE (J)
Davis, Antarctica	34.5
Ascension Island	169.2
SANAE Base, Antarctica	193.9
Perth, Australia	2268.3
Rothera, Antarctica	2413.5
Tel Aviv, Isreal	4701.1
...	...
Honolulu, Hawaii	1.35×10^8
Dunedin, New Zealand	5.09×10^8

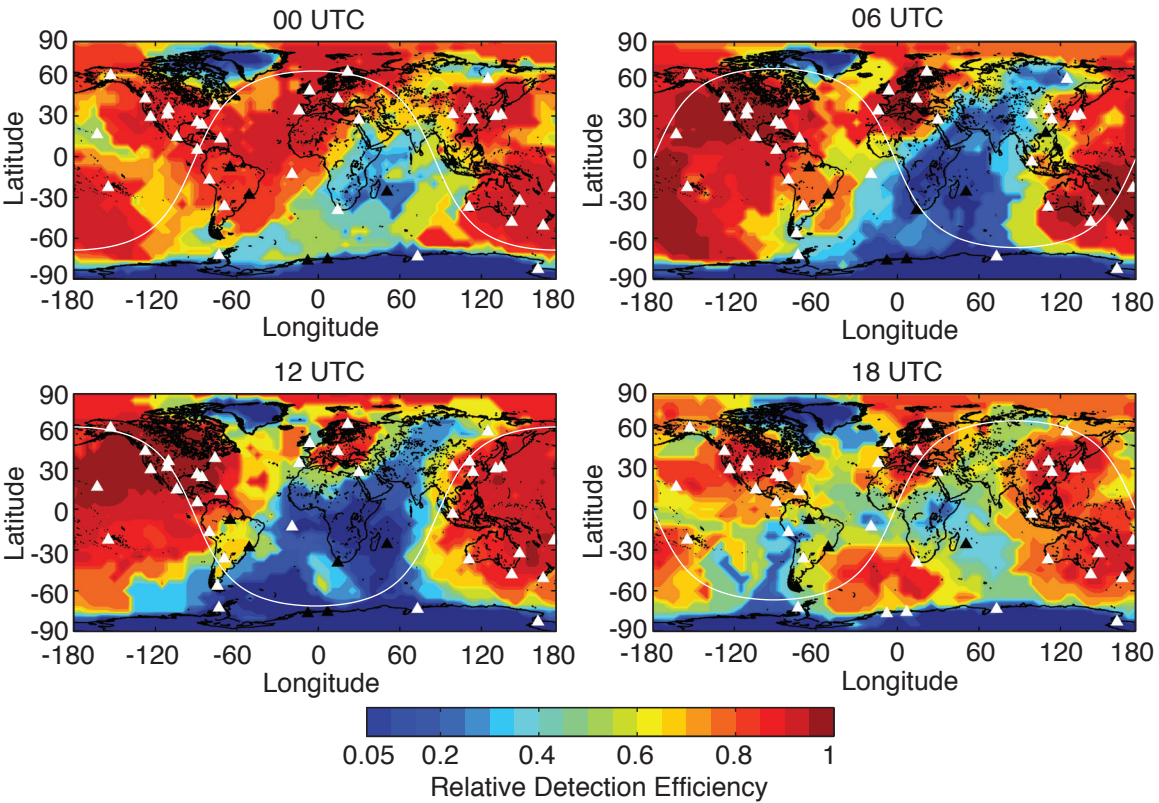


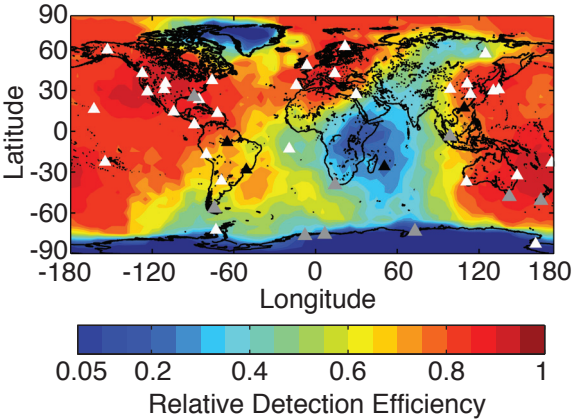


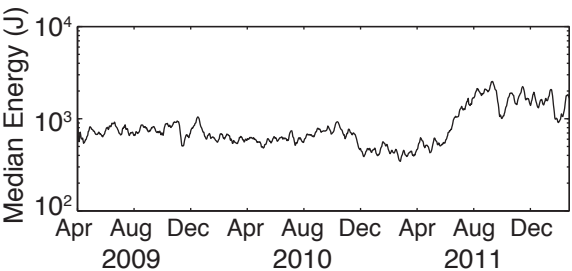








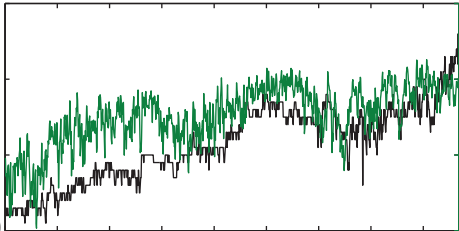




Operational Stations

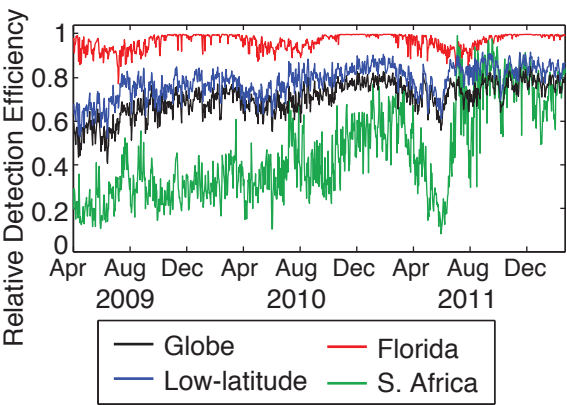
60
50
40
30

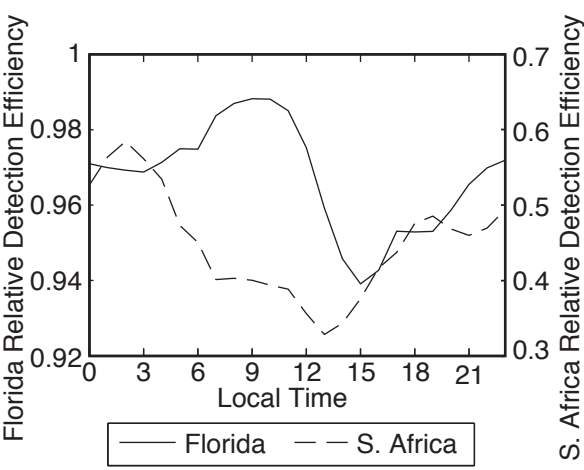
Apr Aug Dec Apr Aug Dec Apr Aug Dec
2009 2010 2011

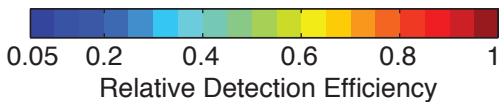
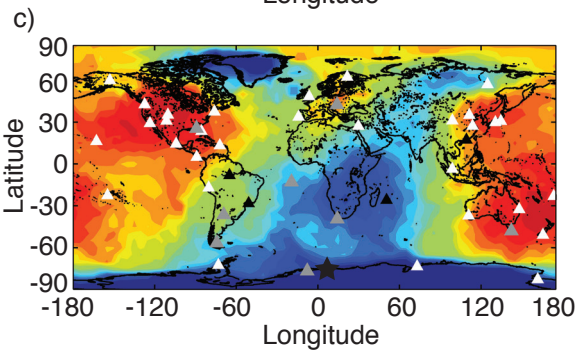
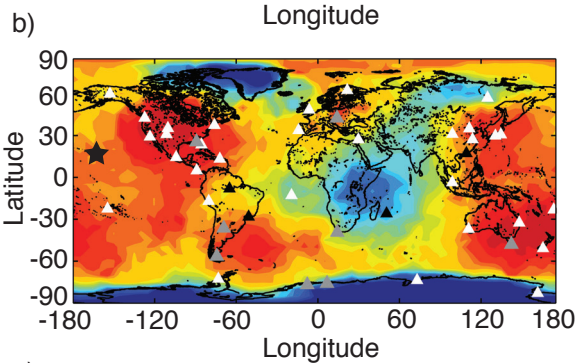
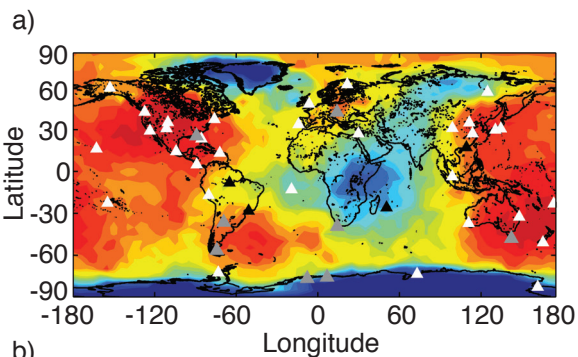


1
0.8
0.6
0.4

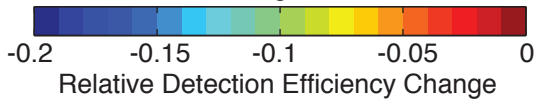
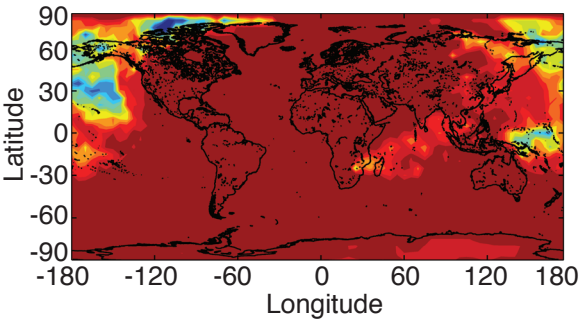
Relative detection efficiency







a)



b)

